Hindawi
Cellular Microbiology
Volume 2023, Article ID 5064371, 14 pages
https://doi.org/10.1155/2023/5064371

Research Article

Mycobacterium avium Infection of Multinucleated Giant Cells Reveals Association of Bacterial Survival to Autophagy and Cholesterol Utilization

Jayanthi J. Joseph,[1] Amy Leestemaker-Palmer,[2] Soheila Kazemi,[2] Lia Danelishvili,[2] and Luiz E. Bermudez[1,2]

[1]*Department of Microbiology, College of Science, Oregon State University, Corvallis, OR, USA*
[2]*Department of Biomedical Sciences, Carlson College of Veterinary Medicine, Oregon State University, Corvallis, OR, USA*

Correspondence should be addressed to Luiz E. Bermudez; luiz.bermudez@oregonstate.edu

Received 27 June 2022; Revised 13 December 2022; Accepted 23 January 2023; Published 11 February 2023

Academic Editor: Jayaprakash Kolla

Mycobacterium avium subsp. *hominissuis* (*M. avium*) is an opportunistic environmental pathogen that typically infects patients with existing lung conditions such as cystic fibrosis or COPD. Pulmonary *M. avium* infection generates peribronchial granulomas that contain infected macrophages and multinucleated giant cells (MGCs). While granuloma formation with MGCs is a common feature of mycobacterial infection, the role of MGCs within the granulomas as well as in the host-pathogen interaction is poorly understood. To shed light on the role of MGCs, we established a novel *in vitro* model utilizing THP-1 cells stimulated with a combination of IFN-γ and TNF-α. In this study, we show that MGCs can take up *M. avium*, which replicates intracellularly before leaving the cell. Bacteria that escape the MGC exhibit a highly invasive phenotype, which warrants further evaluation. Characterization of MGCs with transmission electron microscopy revealed an accumulation of cytoplasmic lipid droplets, autophagic activity, and multiple nuclei. Autophagy markers are upregulated in both uninfected and infected MGCs early in infection, measured by RT-qPCR analysis of Beclin-1 and LC3. Inhibition of autophagy with siRNA significantly reduced *M. avium* survival significantly in THP-1 macrophages. Depletion of host cholesterol and sphingomyelin in MGCs also resulted in decreased survival of *M. avium*. These processes potentially contribute to the formation of a supportive intracellular environment for the pathogen. Collectively, our results suggest that *M. avium* is adapted to replicate in MGCs and utilize them as a springboard for local spread.

1. Introduction

Mycobacterium avium subsp. *hominissuis* (*M. avium*) is an environmental opportunistic pathogen that causes chronic, granulomatous pulmonary infections in patients with underlying lung pathology or immunosuppression [1]. In recent years, the number of *M. avium* infections has been increasing worldwide [2]. Treatment of pulmonary infections involves multiple antibiotics for a minimum of 12 months and is only effective in 50-60% of patients [1, 3]. Airway infections are characterized by the formation of pulmonary lesions, nodules, and both nonnecrotic and necrotic peribronchiolar granulomas [4, 5]. Upon infection, *M. avium* traverses the bronchial epithelium and is phagocytosed by macrophages and circulating monocytes. To sustain a chronic infection, mycobacteria must evade the immune system and find supportive niches to foster bacterial growth and dissemination. One strategy is to survive intracellularly, which *M. avium* accomplishes by inhibiting phagosome acidification, which promotes bacterial survival and replication [6, 7]. There is growing evidence that mycobacteria hijack the host's granulomatous response for their benefit. Traditionally, granulomas were described as protective structures formed by the host immune system to "wall off" pathogenic bacteria and curb dissemination. However, over the past decade, research has shown that mycobacteria can

survive and persist in granulomas [8]. Studies on *Mycobacterium marinum* infection in zebrafish demonstrated that granulomas facilitate cell-to-cell spread, increase bacterial loads, and contribute to dissemination [9, 10]. Additionally, disruption of granulomas in zebrafish can promote host survival as shown in studies performed by Cronan and colleagues, suggesting that granulomatous inflammation is propathogen [11].

Langhans multinucleated giant cells (MGCs) are a characteristic feature of granulomas formed in response to pathogens, rather than foreign materials [12]. MGCs in mycobacterial granulomas contain high bacterial loads *in vivo*, shown by histological examination of granuloma tissues from rabbits, mice, and humans [13–17]. Multinucleated giant cells are formed by the fusion of monocytes and are characterized by multiple nuclei, elevated cholesterol metabolism, and upregulation of iNOS [15, 18]. The interactions between mycobacteria and multinucleated giant cells have not been fully characterized. Previous studies have shown that *M. avium*-induced MGCs are able to take up bacteria [15, 16]. Understanding the role of MGCs in mycobacterial pathogenesis may shed light into the balance of host-pathogen interactions during chronic infection. We developed an *in vitro* model of MGCs to help understand the contribution of MGCs in mycobacterial pathogenesis and the balance of the host-pathogen interaction during chronic infection of *M. avium*.

Lipids are a well-known source of nutrition for mycobacteria in the host [19]. Host lipid metabolism shifts during mycobacterial infections, and the inhibition of lipid accumulation in mycobacterium-infected macrophages reduces bacterial survival [20, 21]. Host lipids utilized by mycobacteria include triacylglycerols, cholesterol, and sphingomyelin. Cholesterol is required for persistence of *Mycobacterium tuberculosis* (*M. tb*) in the lungs of chronically infected mice and *Mycobacterium avium* subsp. *paratuberculosis* in human macrophages [22, 23]. In humans, cholesterol accumulates in *M. tb* granulomas, accompanied by an increase in host lipid metabolism and providing a nutrient-rich environment for mycobacteria [24]. *M. avium* possesses genes involved in cholesterol metabolism, including several *mce* (mammalian cell entry) genes, which are associated with cholesterol uptake and utilization in mammalian hosts [23, 25]. Sphingolipids are important components of eukaryotic cell membranes, and several intracellular pathogens have evolved mechanisms to utilize this class of lipids for growth [26]. Several intracellular pathogens manipulate host sphingolipid metabolism, including *M. tb*, *P. aeruginosa*, and *L. pneumophila* [26]. *M. tuberculosis* possesses several genes involved in cholesterol metabolism, a neutral sphingomyelinase SpmT (Rv0888), and alkaline ceramidase (Rv0669c) [27, 28]. Although *M. avium* lacks homologs for either of these genes, it possesses several uncharacterized hypothetical genes that may have similar activity [23, 25]. For example, *Pseudomonas aeruginosa* uses host sphingomyelin and ceramide as a nutrient by destroying them with a host-mimicking sphingomyelin synthase and ceramidase [29, 30]. *M. tb* utilizes host sphingomyelin by expressing the SpmT (rv0888) gene to support intracellular replication in macrophages [27]. While *M. avium* lacks the SpmT gene, it possesses other genes involved in lipid uptake and degradation, which may play a similar role [25].

In this study, we developed an *in vitro* MGC model and characterized the cellular morphology, which included multiple nuclei, accumulation of cytoplasmic lipid droplets, and the presence of autophagy. We determined the uptake and survival of *M. avium* in MGCs and found that *M. avium* is well adapted at intracellular replication in MGCs. We evaluated the MGC-*M. avium* interaction and identified possible explanations for the contribution of increased host autophagy and cytosolic lipid droplets toward bacterial survival.

2. Materials and Methods

2.1. Bacterial Culture. Mycobacterium avium subsp. *hominissuis* strains 104 (MAH 104), A5 (MAH A5), 101 (MAH 101), and 109 (MAH 109) were originally isolated from the blood of AIDS patients [31]. MAH 101 is the standard *M. avium* strain for susceptibility testing, and MAH 109 has been used extensively in preclinical studies [32]. MAH A5 exhibits prolific biofilm formation and eDNA export [33]. MAH 104 and MAH A5 were grown on Middlebrook 7H10 agar supplemented with 10% *w*/*v* oleic acid, albumin, dextrose, and catalase (OADC, Hardy Diagnostics) for 7-10 days at 37°C.

2.2. Tissue Culture and Formation of Multinucleated Giant Cells. THP-1 (TIB-202) human monocytes were obtained from the American Type Culture Collection (ATCC) and maintained in RPMI 1640 supplemented with 10% heat-inactivated fetal bovine serum (FBS; Gemini Bio-Products) at 37°C with 5% CO_2. THP-1 cells were seeded in 48-well plates at a density of 3.5×10^5 cells per well and differentiated with 50 ng/ml of Phorbol 12-myristate 13-acetate (PMA; Sigma Aldrich) for 24 hours, followed by 24 hours in RPMI 1640 supplemented with 10% FBS without PMA, prior to use in experiments. Differentiated macrophages were treated with IFN-γ (100 ng/ml) (R&D Systems) and TNF-α (25 ng/ml) (VWR). The cytokines were used in combination to promote multinucleated giant cell (MGC) formation. Cytokines in RPMI 1640 supplemented with 10% FBS were added every 48 hours for 6 days after initial PMA treatment triggered differentiation. The fusion index was calculated using the following formula: (No.of nuclei in MGCs)/(total No.of nuclei) × 100%.

2.3. Flow Cytometry. For CD40 surface marker analysis, THP-1 cells were seeded in a 6-well plate (1×10^6 cells/ml) and differentiated with 50 ng/ml PMA for 24 h. MGCs were formed as described above. Cells were detached from the plate using 0.25% EDTA-free trypsin (Thermo Fisher Scientific) in 1X phosphate-buffered saline (PBS) for 5 min at 37°C, followed by gentle pipetting. Cell suspensions were washed with PBS and either left unstained or stained with fluorochrome-conjugated antibodies: CD40 FITC (5C3) (eBioscience) or mouse IgG1 kappa isotype control (P3.6.2.8.1) (eBiosciene) FITC, for 1 hour at 4°C. After staining, cells were fixed with 2% paraformaldehyde (PFA) for

10 min at 37°C to prevent bacterial contamination of the machine, washed, and analyzed immediately. Gating was performed to exclude dead cells. Flow cytometry was performed using an Accuri C6 flow cytometer (BD Biosciences). Data were analyzed using Accuri C6 software, FlowJo, and GraphPad Prism 9.

2.4. Mycobacterial Infection and Survival in MGCs. MAH bacteria were added to multinucleated giant cells at an MOI of 10, synchronized by centrifugation for 10 min at 150 × g, and allowed to infect for 1 hour. Inoculums for these assays were formed in 1X HBSS supplemented with 0.05% Tween-20 (Sigma-Aldrich). Extracellular bacteria were removed by two wash steps with 1X HBBS followed by treatment with gentamicin sulfate (Sigma-Aldrich) for 1 hour (100 μg/ml) and an additional wash step with 1X HBSS to remove the antibiotic and dead extracellular bacteria. Cells were lysed at appropriate time points with 0.1% Triton-X for 10 min, and resulting lysates were diluted and plated. Colony forming units (CFUs) were enumerated at 1, 24, 48, and 72 hours postinfection (h.p.i.). Potential extracellular bacteria escaping from cells were quantified at each time point via spot plating. Briefly, 5 μl of media removed from infected wells was plated on 7H10 agar. Colonies were counted after 7 days of incubation at 37°C.

2.5. Collection of MGC-Passaged Bacteria. MGCs, formed as described previously, were infected with wild-type MAH A5 for 1 h at an MOI of 10. The infection was carried out as described previously. Fresh media were replaced every 24 h. Supernatants were collected at 72 h.p.i, and immediately kept on ice. Cell debris was removed by centrifugation for 5 min, 150 × g at 4°C. The supernatant containing bacteria was pelleted by centrifugation for 15 min, 2000 × g at 4°C. The supernatant was removed, and the pellet resuspended in 2 ml of HBSS and stored at 4°C for up to 7 days before use in experiments.

2.6. qPCR of Autophagy-Associated Genes during MGC Infection. THP-1 and MGC RNA were isolated with the RNeasy mini kit (Qiagen), followed by treatment with DNase I recombinant (Roche Diagnostics) for 2 hours at 37°C to remove contaminating genomic DNA. The DNase was inactivated with Turbo DNase-inactivation reagent (Turbo DNA-free kit, Thermo Fisher Scientific) for 2 min at 37°C. Inactivation reagent was removed via centrifugation for 1 min at 10,000 × g, and RNA transferred to new collection tubes. RNA samples were stored at -4°C for future processing. cDNA was transcribed from host RNA using the iScript cDNA synthesis kit (Bio-Rad). The quality of cDNA was tested by PCR with Gold 360 Master Mix using the manufacturer's specifications (Thermo Fisher Scientific). The RT-qPCR reaction was performed using iQ SYBR Green Supermix (Bio-Rad) and an iCycler (CFX Connect Real-Time Systems, Bio-Rad) as previously described [34]. All gene expression data are presented as relative expression to beta-actin. Primers were designed in Primer3 using sequences from GenBank (National Center for Biotechnology Information). Primer sequences are as follows: beclin-1, 5′-AGCTGCCGTTATACTGTTCTG-3′ (forward) and 5′-ACTGCCTCCTGTGTCTTCAATCTT-3′ (reverse); LC3-II, 5′-GATGTCCGACTTATTCGAGAGC-3′ (forward) and 5′-TTGAGCTGTAAGCGCCTTCTA-3′ (reverse); and beta-actin: 5′-CATGTACGTTGCTATCCAGGC-3′ (forward) and 5′-CTCCTTAATGTCACGCACGAT-3′ (reverse) [35].

2.7. Fluorescent and Transmission Electronic Microscopy of MGCs. Multinucleated giant cells were generated with cytokines in chamber slides (Falcon, VWR) and visualized by fluorescence microscopy. The cells were fixed in 2% PFA for 15 min, washed twice with 1X HBSS, and permeabilized for 10 min with 0.1% Triton-X before staining with 1 μg/ml Hoechst 34580 (Invitrogen) for 15 min in the dark. Hoechst was removed, and samples were washed twice with 1X HBSS and stained with 0.165 μM Alexa Fluor 488 phalloidin (Thermo Fisher Scientific) for 15 min in the dark, followed by two wash steps with 1X HBSS. Slides were allowed to dry before affixing glass coverslips with Cytoseal (Thermo Fisher Scientific). Slides were imaged with a Leica DM4000B fluorescent microscope (Leica Microsystems) and QICAM Fast 1394 camera (QImaging) at a magnification of 1000x under oil immersion. Images were acquired and processed with QCapture Pro 7 software. For TEM, cells were detached from 6-well plates by treatment with 5 mM EDTA for 30 min, washed in 1X HBSS (HBSS, Cellgro), and suspended in fixative buffer with 2.5% glutaraldehyde, 1% formaldehyde, and 0.1 M sodium cacodylate for 24 hours prior to submission to the electron microscopy facility for processing. Samples were sectioned, dehydrated, and visualized by a FEIT Titan 80-200 TEM/STEM microscope at Oregon State University Electron Microscopy Facility.

2.8. siRNA Targeting of Autophagy Genes during Mycobacterial Infection. To examine the role of ATG5 and Beclin-1 in activation of autophagy, we inhibited the functionality of selected targets in THP-1 macrophages using siRNA technology in accordance with the manufacturer's recommendations (Santa Cruz Biotechnology, Inc). THP-1 cells were differentiated and seeded at 80% confluence in 6-well plates and, prior to infection, transfected with ATG5 and Beclin siRNAs. Briefly, siRNAs were diluted in RPMI without serum at a final concentration of 25 nM and 3 μl of Continuum™ transfection reagent (Gemini). Macrophage monolayers were washed once with siRNA transfection medium and replenished with new transfection medium containing target-specific siRNA transfection reagent mixture. Cells were incubated at 37°C in the presence of 0.5% CO_2. Untreated and control siRNA- (nontargeting sequences) transfected cells served as negative controls. After 48 h, monolayers were infected for different time points and lysed and bacterial CFUs were recorded on Middlebrook 7H10 agar plates. Before infection, the ATG5, Beclin, and β-actin protein levels from control and experimental wells were analyzed by semi-quantitative western blotting. Lysed macrophages were resolved by electrophoresis on 12.5% SDS-PAGE gels, transferred to nitrocellulose membranes, and blocked overnight with 5% Bovine Serum Albumin (BSA). After incubation

with primary antibodies at a dilution of 1 : 200 for 2 h, membranes were washed three times with PBS and then probed with corresponding IRDye secondary antibody (Li-Cor Biosciences, Inc) at a dilution of 1 : 5000 for 1 h. Proteins were visualized using Odyssey Imager (Li-Cor).

2.9. Statistical Analysis. All described experiments were repeated at least three times, and data shown are representative of the biological replicates. Comparisons between two groups were analyzed in Microsoft Excel using the two-tailed Student t-test. Results with P values below 0.05 were considered significant.

3. Results

3.1. IFN-γ and TNF-α Induce Multinucleated Giant Cell Formation In Vitro. To trigger *in vitro* MGC formation, THP-1 cells were differentiated with Phorbol 12-myristate 13-acetate (PMA) for 24 hours, followed by stimulation with a combination of TNF-α and IFN-ɣ for 6 days. After differentiation with PMA, THP-1 cells do not proliferate and become adherent. TNF-α and IFN-ɣ were selected because they have been shown to drive granuloma formation and contribute to MGC formation *in vivo* [36–39]. A fusion index of 56.5% was observed when cells were treated with 25 ng/ml TNF-α and 100 ng/ml IFN-ɣ over a 6-day period (Figure 1(a)). The resulting mixed population of MGCs and activated THP-1 macrophages was utilized for further experiments. MGCs formed with this protocol have 2-4 nuclei (Figures 1(b)–1(d)). CD40 is a marker of MGCs associated with mycobacterial infection and is involved in MGC formation [40, 41]. MGCs exhibited a significant shift in mean fluorescent intensity (MFI) of FITC-CD40, indicating that 98% of MGCs are CD40 positive (Figure 1(e)). THP-1 cells exhibited a small shift in fluorescent intensity, indicating a low percentage of CD40-positive cells (Figure 1(f)). MGCs have an MFI of FITC-CD40 that is significantly higher than THP-1 macrophages, MGCs stained with a FITC-isotype control, and unstained MGCs (Figure 1(g)). These results indicate that MGCs retain the CD40 marker and are biologically similar to MGCs observed *in vivo*.

3.2. Intracellular Survival and Growth of M. avium in Multinucleated Giant Cells. The intracellular stages of mycobacteria in MGCs have not been fully described. Survival assays were performed to characterize the uptake and intracellular growth of *M. avium* in the *in vitro* MGC model and compared to THP-1 macrophages. *M. avium* A5 infected MGCs at a similar rate to THP-1 macrophages (Figure 2(a)). Once cells were infected, bacterial survival was determined by CFU counts in either MGCs or THP-1 macrophages over 3 and 6 days, respectively, and fold change relative to 1 h.p.i calculated. The time points selected for THP-1 survival assays are standard practice. The time points for MGC survival assays were selected from day 5 of stimulation up to the point where bacterial growth was observed at 3 d.p.i. Additionally, by 6 d.p.i, the MGCs would have been on the plate for 12 days, which would reduce the number of viable cells. At 4 d.p.i for THP-1 and 48 h.p.i for MGC, fold change of bacterial growth was 4 (Figures 2(b) and 2(c)). In THP-1 macrophages, *M. avium* intracellular growth exhibited a fold change of 11 at 6 d.p.i, whereas *M. avium* intracellular growth in MGCs exhibited a fold change of 7 at 3 d.p.i (Figures 2(b) and 2(c)). During the survival assay, CFU/milliliter of extracellular bacteria that exited MGCs was enumerated (Figure 2(d)). The number of bacteria leaving MGCs was significantly greater at 72 h.p.i. compared to other time points. These data indicate that *M. avium* A5 can enter MGCs with the same efficacy as THP-1 macrophages. Additionally, *M. avium* A5 survives in the MGC environment and shows a similar growth trend to THP-1 macrophages. Our data support the idea of a favorable niche existing inside the MGC environment that *M. avium* A5 can utilize to survive and eventually leave to infect other cells nearby.

3.3. Characterization of M. avium Phenotype upon Leaving Multinucleated Giant Cells. To determine if the phenotype of MGC-passaged *M. avium* A5 is different than WT *M. avium* A5, uptake and survival assays were carried out in THP-1 macrophages. To passage *M. avium* A5, MGCs were infected with WT *M. avium* A5 for 1 h, and at 72 h.p.i, bacteria that exited the MGCs (MGC-passaged A5) were collected in cell culture media and kept on ice or at 4°C while being pelleted and washed. THP-1 cells were infected for 1 hour with MGC-passaged bacteria or *M. avium* A5 from a 7H10 streak plate. Uptake of *M. avium* A5 was evaluated by inhibiting macropinocytosis and receptor-mediated phagocytosis. Wortmannin inhibits the macropinocytosis pathway by preventing complete closure of the cytoplasmic ruffles. Blocking complement receptor 3 (CR3) with a CD11b antibody inhibits complement receptor-mediated phagocytosis. MGC-passaged A5 exhibited a percent uptake approximately 3 times greater than *M. avium* A5 grown on a plate, under normal infection conditions (Figure 3(a)). Blocking the CR3 receptor with an anti-CD11b antibody for 1 hour prior to infection led to a 52% reduction in uptake for both bacterial phenotypes (Figure 3(b)). Inhibition of macropinocytosis with wortmannin for 2 h prior to infection led to a 33% reduction in uptake for both bacterial phenotypes (Figure 3(b)). Inhibiting uptake pathways reduced the uptake of both phenotypes but did not completely block them, showing that *M. avium* of either phenotype can circumvent the effect of the inhibitors and entering the macrophage via an alternate route. This suggests that MGC-passaged bacteria can enter THP-1 cells via alternate routes. Survival in THP-1 macrophages over 6 days with MGC-passaged A5 is comparable to A5 from the plate; thus, once bacteria invade macrophages, there was no added advantage to MGC-passaged bacteria (Figure 3(c)). These data suggest that the MGC environment increases the invasiveness of *M. avium* A5 but that they retain their ability to enter the next host cell in multiple ways.

3.4. Electron Microscopy Observations of M. avium A5 in MGCs. To increase our understanding of the behavior of bacteria inside MGCs, transmission electron microscopy (TEM) was used. MGCs were infected with *M. avium* over 72 h then processed for TEM. THP-1 macrophages that are

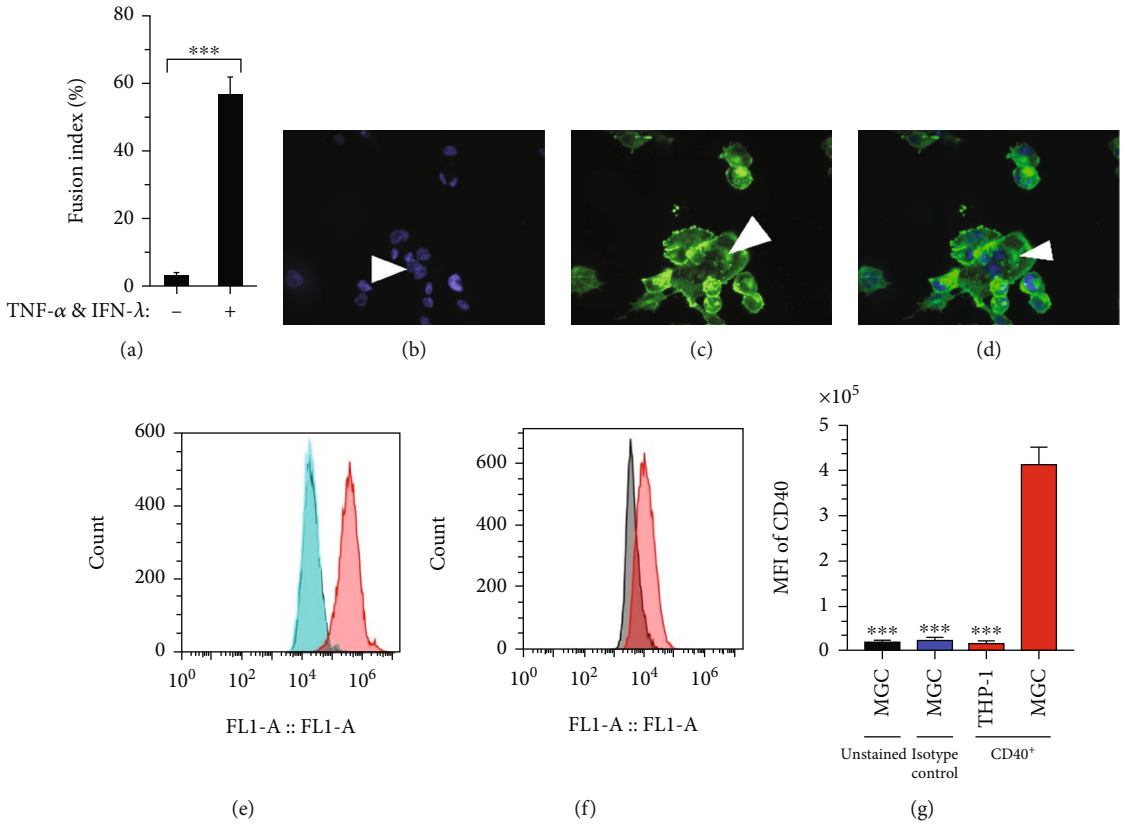

FIGURE 1: IFN-γ and TNF-α induce formation of multinucleated giant cells *in vitro*. THP-1 cells were fluorescently labeled after cytokine treatment to determine MGC formation via microscopy at 1000x magnification. The expression of CD40, a marker associated with classical macrophage activation and Langhans giant cells, was measured via flow cytometry. (a) The macrophage fusion index determined the percentage of multinucleated cell having at least 3 nuclei in 10 fields of view. (b) Hoechst stain of MGC nuclei (white arrow). (c) Alexa Fluor Phalloidin 488 stain of actin cytoskeleton (white arrow). (d) Merged image of MGC (white arrow). (e) FITC-CD40 levels in MGCs (black: unstained, blue: isotype control, and red: $CD40^+$). (f) FITC-CD40 levels in PMA-differentiated THP-1 cells (black: unstained, red: $CD40^+$). (g) Mean fluorescent intensity of FITC-CD40 (black: unstained, blue: isotype control, and red: $CD40^+$). All groups were compared to MGC $CD40^+$. Data are representative of 3 independent experiments. Statistical comparisons: $^*P < 0.01$, $^{**}P < 0.001$, and $^{***}P < 0.0001$.

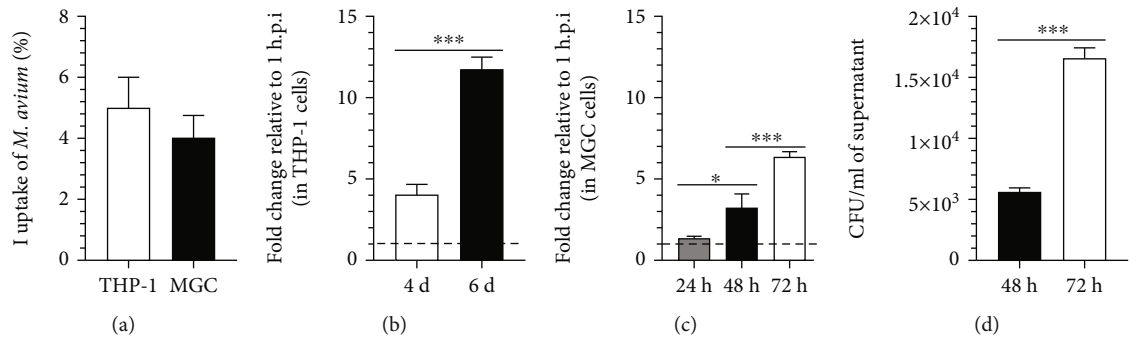

FIGURE 2: Infection and survival of *M. avium* A5. (a) Percent uptake of *M. avium* A5 in THP-1 macrophages and MGCs after 1 hour of infection. (b) Fold change relative to 1 h.p.i (dashed line) of *M. avium* growth over 6 days in THP-1 macrophages. (c) Fold change relative to 1 h.p.i (dashed line) of *M. avium* growth over 3 days in MGCs. (d) Extracellular bacterial CFUs recovered after infection of MGCs. Data shown are representative of results from three independent biological replicates. Statistical comparisons: $^*P < 0.05$; $^{**}P < 0.005$; $^{***}P < 0.0005$.

not treated with cytokines or infected with bacteria show normal cellular structures including a single nucleus and cell size. After cytokine exposure, MGCs were formed and autophagosomes were visible in the cytosol, characterized by double membranes (Figure 4(a)). In MGCs infected with *M. avium* A5 for 72 h, bacteria can be seen inside autophagosomes (Figure 4(b)), and bacterium-containing vacuoles can be seen interacting with autophagosomes (Figures 4(c) and

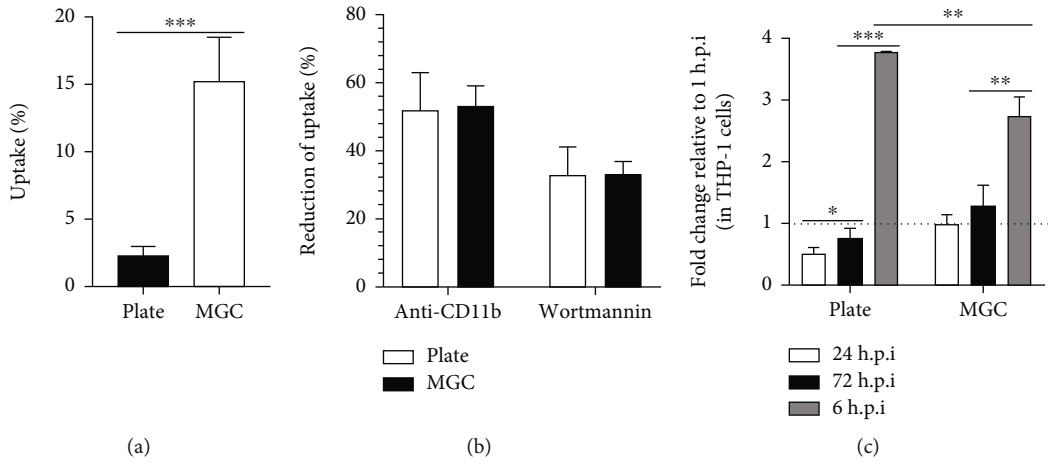

FIGURE 3: Uptake and survival of MGC-passaged *M. avium* A5 in THP-1 cells. (a) Percent uptake of *M. avium* A5 inoculums in THP-1 cells after 1 h of infection. (b) Percent reduction of uptake by THP-1 cells treated with either wortmannin for 2 h or a CD11b antibody for 1 h, prior to infection. (c) Fold change relative to 1 h.p.i (dashed line) of bacterial survival by plate or MGC-passaged *M. avium* in THP-1 macrophages over 6 days. "Plate" refers to *M. avium* A5 grown on a 7H10 plate, and "MGC-passaged" refers to *M. avium* A5 that was collected from infected-MGCs at 72 h.p.i. Data are representative of three independent experiments. Statistical comparisons: $^{*}P < 0.01$, $^{**}P < 0.001$, and $^{***}P < 0.0001$.

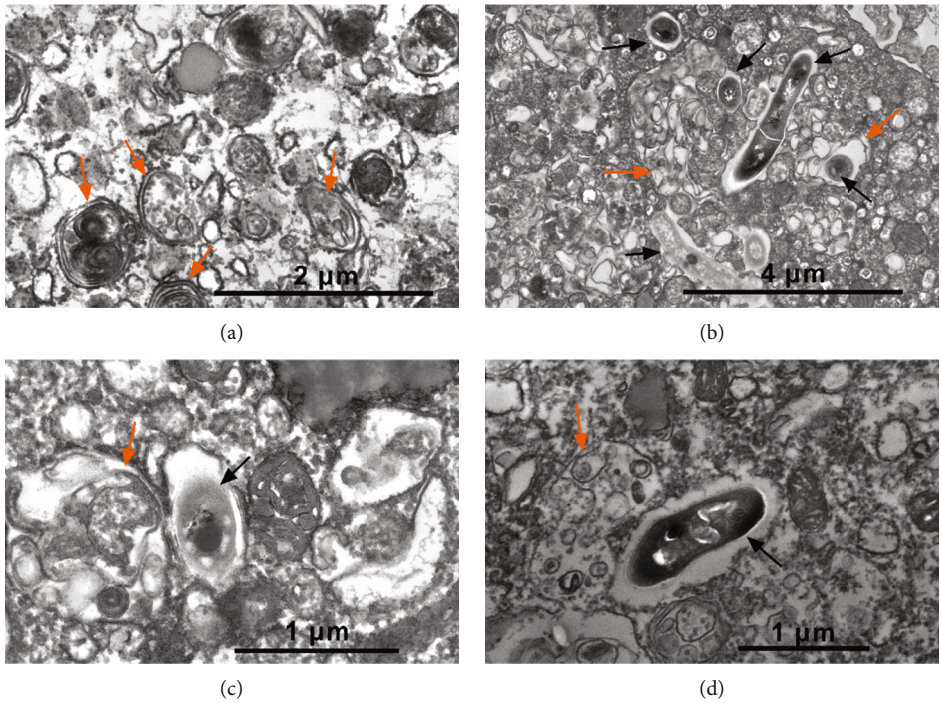

FIGURE 4: Autophagic activity in MGCs. (a) Autophagosomes containing cellular components in uninfected MGCs. (b) Autophagosomes containing *M. avium* 72 h.p.i. of MGCs. (c) Vacuoles containing *M. avium* interacting with an autophagosome at 72 h.p.i. (d) Same as (c). Black arrows: bacteria; orange arrows: autophagosomes.

4(d)). Comparing multiple cells, numerous autophagic vacuoles exist within MGCs, and once these cells are infected with *M. avium* A5, the number of autophagosomes increased substantially.

The formation of MGCs causes several cellular changes, and one of the changes observed was the accumulation of lipid droplets in the cytosol (Figure 5(a)). At 1 h.p.i, bacteria were present the cytosol near lipid droplets (Figure 5(b)) as well as in autophagosomes (Figures 5(c) and 5(e)). Intracellular lipid inclusions were present in intracellular bacteria at several time points (Figures 5(b)–5(e)). Vacuoles with multiple bacteria were observed at 72 h.p.i. (Figure 5(d)). After 24 h, bacteria started to leave MGCs and were observed near the plasma membrane (Figure 5(f)).

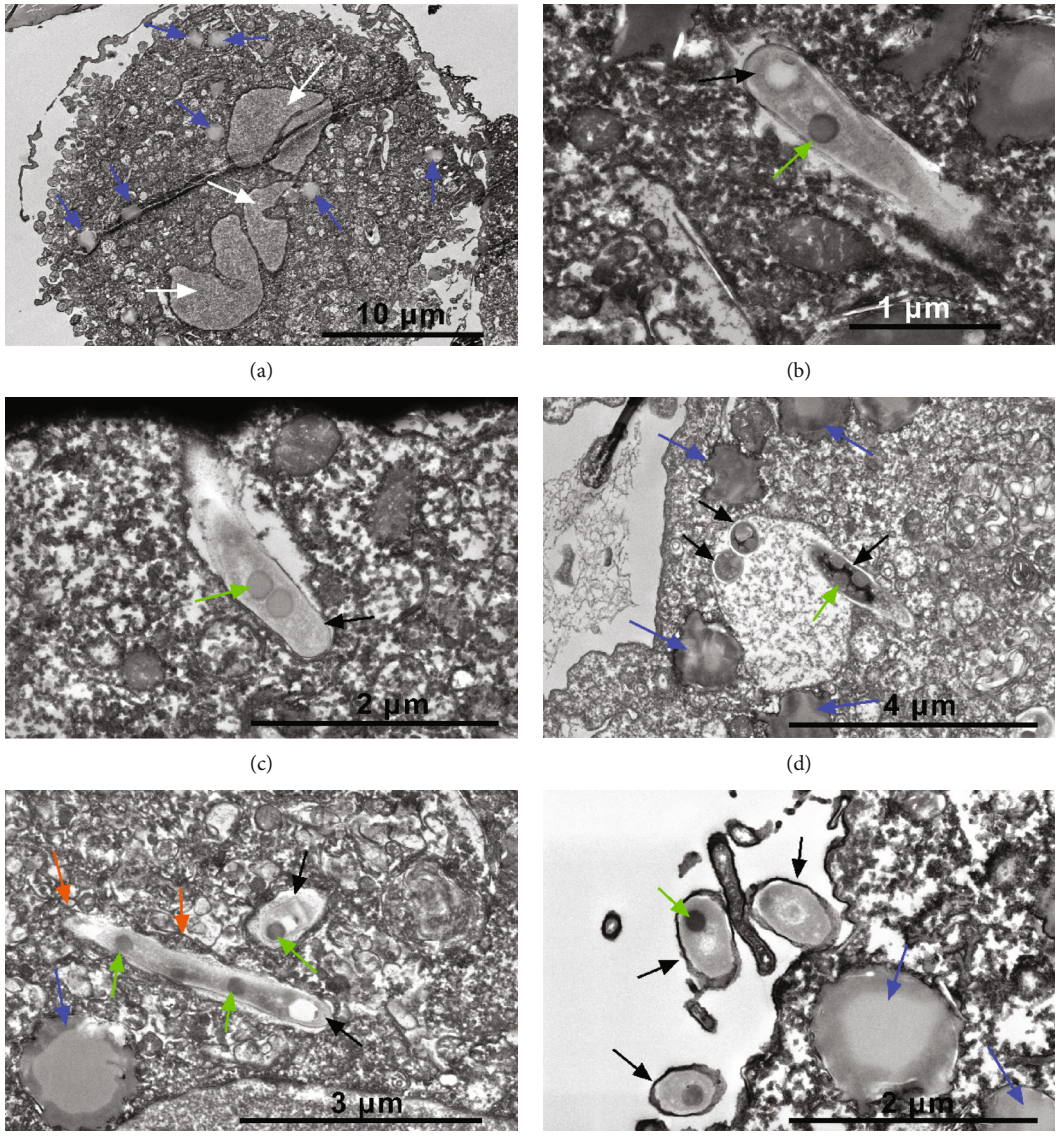

Figure 5: Characteristics of intracellular *M. avium* in MGCs. (a) Uninfected MGC with three nuclei surrounded by lipid droplets. (b) Cytosolic M. avium inside MGCs at 1 h.p.i. (c) *M. avium* bacterium in a vacuole at 1 h.p.i in MGCs. (d) Vacuole containing multiple M. avium 72 h.p.i. inside MGCs. (e) Intracellular M. avium in autophagosome in MGC at 1 h.p.i. (f) 24 h.p.i., extracellular *M. avium* from an MGC. Blue arrows: host lipid droplets, black arrows: bacteria, green arrows: intrabacterial lipid inclusions, white arrows: nuclei, and orange arrows: autophagosomes.

3.5. In Vitro Multinucleated Giant Cells Exhibit Increased Autophagic Activity Compared to Macrophages. To assess autophagic activity in MGCs, we quantified mRNA levels of LC3 and Beclin-1 via real-time PCR. Beclin-1 controls phagophore formation, and LC3 is involved in phagophore elongation [42]. Beclin-1 gene levels after 4 h indicate that MGCs have naturally greater expression compared to THP-1 macrophages, and once infected, MGCs exhibited even greater gene expression of Beclin-1 (Figure 6(a)). The trend continued through 24 h.p.i, except there was no difference between infected and uninfected MGC gene expression. Later in the infection, there was no difference in Beclin-1 gene expression between experimental groups. LC3 expression by MGCs at 4 h showed significant increase compared to LC3 expression by THP-1 macrophages (Figure 6(b)). After 24 h, LC3 gene expression by uninfected MGCs increases, and expression by infected MGCs decreased. This could be due to suppression of autophagic flux by *M. avium*, which has been demonstrated in *M. abscessus* [43]. After 72 h, LC3 gene expression was undetectable for all experimental groups. The reduction in autophagic marker expression by 72 h.p.i could be due to the absence of cytokine stimulation after the start of infection. For infected MGCs, the reduction could be due to bacterial exit from the cell.

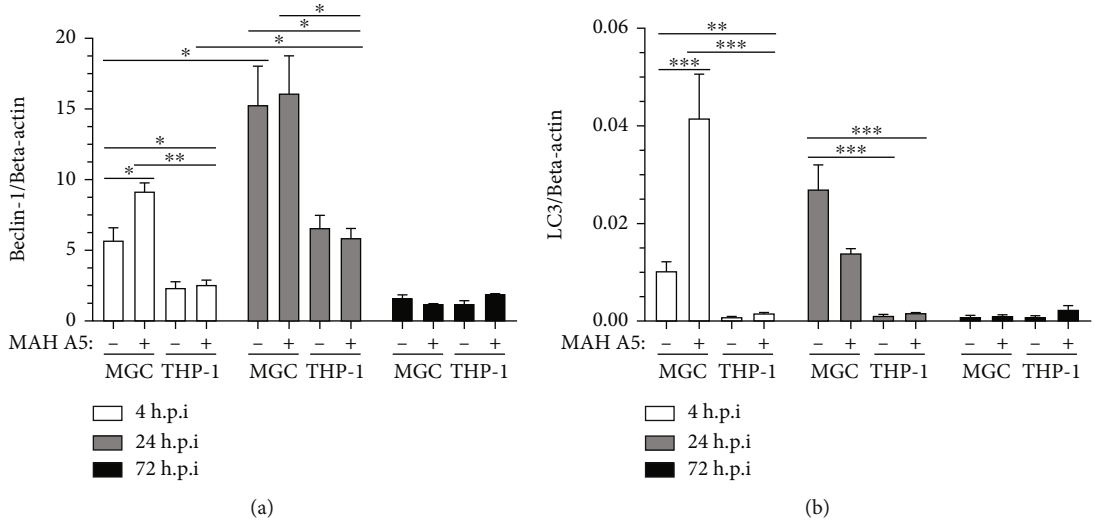

Figure 6: Gene expression of autophagic markers is elevated in MGCs. Either MGCs or THP-1 cells were infected with WT *M. avium* A5 for 4 h. (a) Beclin-1 transcripts were measured by RT-qPCR at indicated times. mRNA levels are presented as relative expression to actin. (b) LC3 transcripts were measured at indicated time points. mRNA levels are represented relative to actin expression. Data are representative of two independent experiments. Statistical comparisons: $^{*}P < 0.01$; $^{**}P < 0.001$; $^{***}P < 0.0001$.

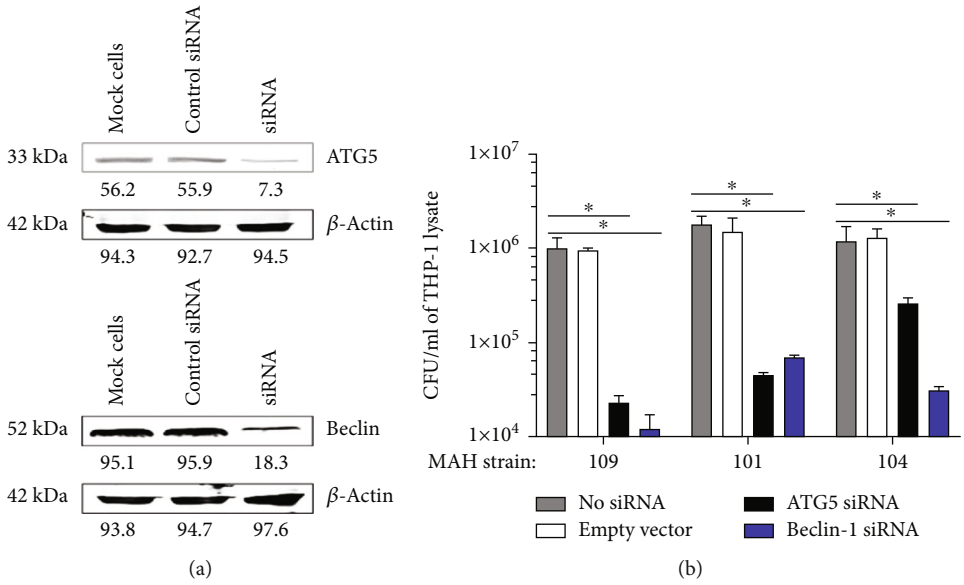

Figure 7: siRNA targeting of autophagy markers decreases protein levels. THP-1 cells were depleted of either ATG5 or Beclin-1 48 h after siRNA targeting. (a) Western blot band intensities were quantified using β-actin as a loading control by Odyssey imager software (Li-Cor). (b) Survival of MAH strains 109, 101, and 104 at 48 h.p.i. in THP-1 macrophages transfected with ATG5 or Beclin-1 siRNA. CFU/milliliter of data is representative of three experiments. Statistical comparisons: $^{*}P < 0.01$; $^{**}P < 0.001$; $^{***}P < 0.0001$.

Collectively, these data support our earlier observation that infected MGCs have a greater number of autophagosomes than uninfected MGCs at early time points.

3.6. Silencing of Beclin and ATG5 Reduces Intracellular Survival of M. avium in THP-1 Macrophages. Since there is a clear tendency of MGCs cells to express autophagy upon *M. avium* infection, which is similar to what is observed at later time points in macrophages, we questioned if autophagy was an important occurrence for survival in host cells. Macrophages, the preferred cell type of *M. avium* and precursor of MGCs, were selected for this experiment. To assess the importance of autophagy during *M. avium* infection in THP-1 macrophages, siRNA technology was used to knock down expression of Beclin-1 and ATG5 host genes. THP-1 macrophages treated with siRNA targeting either Beclin, ATG5, empty vector, or no vector showed reduced but not absent protein levels inside of cells, confirmed by western blot (Figure 7(a)). These THP-1 macrophages were then infected with multiple strains of *M. avium* including 101, 104, and 109. Our results demonstrate that inhibition of ATG5 or Beclin, markers of autophagy, decreased the ability

for bacteria to survive in macrophages over 4 days (Figure 7(b)). These data suggest that *M. avium* uses autophagy for intracellular survival in resting macrophages. It is possible that the autophagic activity in MGCs aids bacterial survival by a similar mechanism.

3.7. Intracellular Cholesterol Transport and M. avium A5 Survival in MGCs. M. avium is clearly utilizing host lipids in MGCs, as shown by the presence of intrabacterial lipid inclusions (Figures 4(b), 5(b), and 5(c)). To determine whether *M. avium* A5 utilizes MGC-derived cholesterol as a source of nutrients for intracellular growth, uptake and survival assays were carried out in MGCs treated with (3β)-3-[2-(diethylamino) ethoxy] androst-5-en-17-one hydrochloride (U18666A), an intracellular cholesterol transport inhibitor. The final concentration was chosen based on previously published studies in mouse macrophages and human fibroblasts [44, 45]. To rule out direct bacterial inhibition, a growth curve of *M. avium* A5 in 7H9 broth supplemented with 3 μg/ml of U18666A was conducted (Figure 8(a)). U18666A had no effect on the growth of *M. avium* A5 over 6 days (Figure 8(a)). Since U18666A did not affect bacterial growth, we then used the inhibitor on MGCs infected with *M. avium* A5. U18666A was added 1 hour after infection of MGCs and replenished daily over 72 h. MGCs were lysed, and CFUs were counted at 1, 24, and 72 h.p.i. In MGCs that were infected with *M. avium* A5, treatment with U18666A did not affect whether bacteria were taken up by the cells (Figure 8(b)). *M. avium* A5 intracellular growth over 72 h was significantly hindered by U18666A compared to without inhibition, with a reduction of about 25% (Figure 8(b)). This indicates that *M. avium* can utilize alternate sources of energy if cholesterol is unavailable in host cell during early stages of infection. However, *M. avium* is unable to overcome the lack of cholesterol later in infection and intracellular growth plateaus. Since the inhibition of intracellular cholesterol transport with U18666A reduces but does not prevent intracellular growth of *M. avium*, we propose that cholesterol is not essential for intracellular growth.

3.8. Effect of Sphingomyelin Synthase Inhibition on M. avium A5 Survival in MGCs. Since sphingomyelin has been shown to be advantageous for TB in macrophages, we determined whether *M. avium* A5 utilizes sphingomyelin in MGCs to aid intracellular growth [27]. MGCs were either treated with tricyclodecan-9-yl-xanthogenate (D609) or untreated. D609 is an inhibitor of sphingomyelin synthase that reduces intracellular diacylglycerol and sphingomyelin and increases ceramide levels [46–48]. D609 was added to infected MGCs 1 hour postinfection and was replenished daily over the course of three days (Figure 8(c)). The concentration of 100 μM was chosen based on previously established inhibitory concentrations in human lung fibroblast and monocyte cell lines [46, 47]. 100 μM of D609 had no effect on the growth of *M. avium* A5 in 7H9 broth after 4 days of growth (Figure 8(a)). To account for the effects of D609 on bacterial growth at day 6, all in vitro experimental time points were determined by day 3. MGCs were infected then lysed, and CFUs were counted at 1, 24, and 72 h.p.i. In MGCs that were treated with 100 μM of D609, uptake of *M. avium* A5 was not affected as D609 was added after infection. *M. avium* A5 intracellular growth was significantly hindered with treatment only at 72 h.p.i, with a reduction of about 30% (Figure 8(c)). This indicates that during early stages of infection, *M. avium* can utilize alternate sources of energy if sphingomyelin is unavailable in the host cell.

To determine the effect of sphingomyelin synthase inhibition after the infection had been more established, MGC survival assays were conducted in which D609 was added to the cells at either 24 h.p.i or 48 h.p.i (Figure 8(d)). When D609 was added to *M. avium* A5-infected MGCS at 24 h.p.i, there was a reduction in bacterial survival at 48 h.p.i. However, *M. avium* A5 was able to overcome the effect of the inhibitor and resumed growth, which is shown by the increase in CFUs from 48 to 72 h.p.i. When D609 was added to *M. avium* A5-infected MGCS at 48 h.p.i, there was a reduction in bacterial survival at 72 h.p.i. The number of extracellular bacteria leaving the MGCs was counted for untreated, 24 h D609, and 48 h D609 groups (Figure 8(e)). In both the untreated and 24 h D609 groups, the number of extracellular bacteria increases between 48 and 72 h.p.i; however, the 48 h D609 group shows no increase during this period. Our results show that *M. avium* A5 can overcome sphingomyelin depletion when it occurs at 24 h.p.i, but not 48 h.p.i., and suggest *M. avium* dependency on sphingomyelin at later stages of infection.

4. Discussion

Multinucleated giant cells play a significant role in the host-pathogen interaction during the granulomatous response to mycobacteria. Past studies have used *in vitro* multinucleated giant cell models that utilize mycobacteria or mycobacterial components and a combination of primary lymphocytes and macrophages to trigger the formation of cellular aggregates with few MGCs [49–51]. The MGC model described in this study focuses on a single cell type, avoiding the use of bacterial components and complexities of cell-aggregate models (formed with several cell types) to detail characteristics of MGCs in the absence of confounding bacterial factors. The absence of bacterial components allows this model to have broader applications beyond mycobacterial studies. In addition, the model utilizes an immortalized cell line, rather than primary cells; this makes it affordable and reproducible. Foreign body multinucleated giant cell models induce macrophage fusion with IL-4 stimulation; however, these MGCs are typically found near medical implants and biomaterials and are significantly different than MGCs found in mycobacterial granulomas [52, 53]. In addition, MGCs formed in this model have the CD40 surface marker, which is present during acute tuberculosis infection and is required for MGC formation in tuberculosis [40, 41].

MGCs are a common feature of mycobacterial granulomas *in vivo* and typically contain large bacterial loads [14–17]. It is not clear whether MGCs play a host-protective role or act in favor of the pathogen. In previous studies, MGCs have been shown to exhibit increased phagocytic activity compared to macrophages [15, 54, 55]. Recent

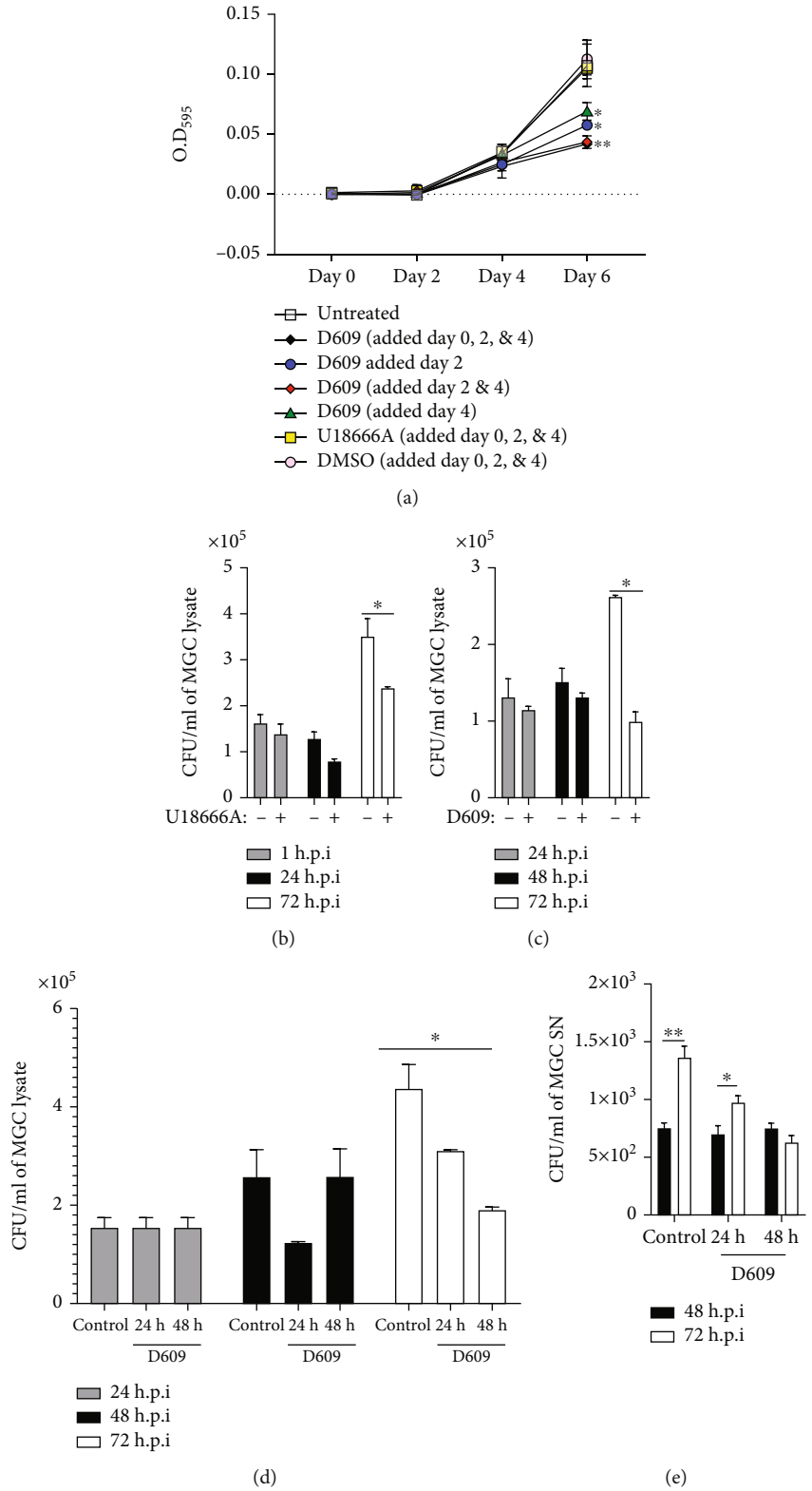

Figure 8: Effects of altering lipid cellular components during mycobacterial infection. (a) Growth curve of *M. avium* A5 in 7H9 supplemented with either DMSO, U18666A (3 μg/ml), or D609 (100 μM). D609 was added at specified time points after inoculation of growth media. (b) Survival of *M. avium* in MGCs in the presence of intracellular cholesterol transport inhibitor U18666A (3 μg/ml) or in media only. (c) Survival of *M. avium* in MGCs in the presence of sphingomyelin synthase inhibitor D609 (100 μM) or in media only. (d) D609 was added to MGCs at 24 or 48 h.p.i.; then, CFUs were determined over 72 h. (e) Extracellular CFUs from (d) supernatants (SN) from infected MGCs were plated at each time point. Statistically significant treatments are compared to untreated. Data shown are from 3 independent experiments. Statistical comparisons: $^{*}P < 0.01$; $^{**}P < 0.001$.

research by Gharun and colleagues supports the idea that MGCs are permissive to mycobacterial replication [15]. In this study, we demonstrated that MGCs formed by the fusion of macrophages after IFN-γ and TNF-α stimulation can phagocytose *M. avium* and allow intracellular replication. Additionally, *M. avium* that leaves the MGC after 3 days exhibits a highly invasive phenotype. Previous work by Early and colleagues have shown that macrophage-passaged *M. avium* exhibits a more invasive phenotype than plate-grown *M. avium* [56]. Their work shows that macrophage-passaged *M. avium* enters uninfected macrophages primarily via macropinocytosis rather than complement receptor-mediated phagocytosis, which is the typical pathway [56]. Our work shows that blocking macropinocytosis significantly reduces the uptake of macrophages by MGC-passaged *M. avium*. These findings also indicate that the MGC environment increases the invasiveness of *M. avium* and that MGC-passaged bacteria can enter macrophages in multiple ways. Previous studies by Clay and colleagues, in the *M. marinum* zebrafish model, demonstrated that infected macrophages control the bacterial burden, migrate into tissues, and recruit additional cells to form granulomas in early stages of infection [57]. Additionally, granulomas themselves facilitate cell-to-cell spread of bacteria and increase bacterial burden [9, 10]. Our finding that *M. avium* exits MGCs and exhibits a highly invasive phenotype suggests that the intracellular environment of MGCs may enhance and contribute to the bacterial replicative niche and drive cell-to-cell spread.

After infection, *M. avium* survives in a cytoplasmic vacuole of macrophages and prevents the acidification and vacuole fusion with lysosomes [58]. The lack of Rab7 marker on *M. avium* late phagosomes influences the phagolysosome fusion [59]. Furthermore, intracellular *M. avium* is resistant to ROS and nitric oxide and capable of subverting macrophage killing mechanisms [60]. Presumably, *M. avium* uses similar strategies for survival in MGCs.

In some cases, autophagy is used as a mechanism to kill intracellular pathogens, such as *Salmonella enterica* serovar *Typhimurium* and *M. tuberculosis* [61, 62]. However, some bacterial species have strategies to avoid autophagic clearance, while others utilize autophagy to fuel intracellular growth or to drive their escape from the host cell [63, 64]. For instance, *Francisella tularensis*, an intracellular pathogen that infects macrophages, exploits autophagy to amass nutrients for intracellular growth [65]. *M. tuberculosis* suppresses macrophage autophagy through the inhibition of production of reactive oxygen species (ROS) [62]. *Mycobacterium marinum*, a model organism for *M. tuberculosis*, employs host autophagic machinery for cell-to-cell transmission of bacteria and is able to prevent maturation to autophagolysosomes [66]. Our work demonstrates that the inhibition of autophagy using RNAi in THP-1 cells leads to a significant reduction in intracellular survival of *M. avium*. Altogether, data collected on the increased autophagy in MGCs, the presence of *M. avium* in autophagosomes, and the permissiveness for bacterial growth suggest that *M. avium* utilizes autophagy to fuel intracellular growth in both macrophages and MGCs.

When we inhibited intracellular cholesterol transport in MGCs, *M. avium* survival was significantly reduced at 72 h.p.i. These data indicate that cholesterol is not vital for intracellular survival and that *M. avium* is able to overcome the lack of cholesterol and replicate in MGCs. Work from Knight et al.'s group has indicated that accumulation of lipids in *M. tuberculosis*-infected macrophages is not triggered by the bacteria but by the host [67]. These findings agree with our observation that *M. avium* makes use of the cholesterol only because it is available; however, it does not affect bacterial survival if cholesterol is limited or absent. Depletion of host sphingomyelin with D609 during *M. avium* infection at different time points temporarily reduced bacterial intracellular growth in MGCs. *M. avium* was able to resume intracellular growth 24 hours after each D609 treatment, indicating that it may use host lipids as an energy source if they are present but can utilize alternative sources of energy if host lipids are not available. Improving our understanding of the role of host lipids in intracellular replication is an important avenue of future research. Characterization of MGC lipid droplets by lipidomics would provide further information about the MGC model and might point to specific lipids utilized by intracellular bacteria.

M. avium that leaves the MGCs readily enters neighboring macrophages. Previous work by Early and colleagues has shown that macrophage-passaged *M. avium* exhibit higher uptake and induces apoptosis in macrophages as a mechanism of cell exit [56]. Apoptosis was not observed during visual inspection of macrophages infected with MGC-passaged *M. avium*. To follow up, an experiment is to measure apoptosis with an Annexin V assay is necessary to confirm this observation. The study published by Early et al. shows that macrophage-passaged *M. avium* enters uninfected macrophages primarily via macropinocytosis rather than complement receptor-mediated phagocytosis, which is the typical pathway [56]. Our work demonstrates that blocking macropinocytosis or complement receptor-mediated phagocytosis significantly reduces the uptake of macrophages by MGC-passaged *M. avium*, suggesting that this phenotype uses multiple routes of entry. The precise escape mechanism of *M. avium* from MGCs remains unclear. *M. marinum* utilizes autophagy to escape from host macrophages in a nonlytic mechanism [68]. *M. avium* may utilize a similar autophagy-mediated pathway of cell exit. Together, these findings demonstrate that exposure to the MGC environment increases the uptake of *M. avium*, by naïve macrophages which may help minimize the time spent in the extracellular space and maximize transmission. Further work is needed to describe the precise mechanism utilized by *M. avium* to exit MGCs.

Previous studies by Clay and colleagues, in the *M. marinum* zebrafish model, demonstrated that infected macrophages control the bacterial burden, migrate into tissues, and recruit additional cells to form granulomas in early stages of infection [57]. Additionally, granulomas themselves facilitate cell-to-cell spread of bacteria and increase bacterial burden [9, 10]. Our finding that *M. avium* exits MGCs and exhibits higher uptake suggests that the intracellular environment of multinucleated giant cells may enhance

and contribute to the bacterial replicative niche and drive cell-to-cell spread. Characterizing the cell exit mechanism utilized by MGC-passaged *M. avium* is an important future direction. Probing the involvement of autophagy on bacterial cell exit would be a good starting point.

Using the *in vitro* model established in this study, we characterized some of the interactions between MGCs and *M. avium*. Bacterial survival assays in MGCs confirm a favorable intracellular environment promoting *M. avium* growth and escape. We also demonstrated that autophagy is elevated in MGCs, and its inhibition reduces *M. avium* survival in phagocytic cells. *M. avium* also appears to utilize host cholesterol and sphingomyelin to fuel intracellular growth. Further study is needed to define the role of lipids versus autophagy in nutrient acquisition by intracellular *M. avium*. Our data indicate that while *M. avium* is well adapted to replicate in MGCs, the host environment stimulates the uptake of bacteria and efficient escape from phagocytic cells likely for local spread.

Data Availability

All the data and microbes are available upon request.

Conflicts of Interest

The authors declare that they have no conflicts of interest.

Authors' Contributions

JJ performed and designed experiments and prepared the manuscript. AP designed experiments and prepared the manuscript. SK performed flow cytometry. LD performed siRNA experiments and edited the manuscript. LB designed experiments, performed siRNA experiments, and edited the manuscript.

Acknowledgments

This work was supported by a grant from the SF Microbiology Foundation.

References

[1] D. E. Griffith, T. Aksamit, B. A. Brown-Elliott et al., "An official ATS/IDSA statement: diagnosis, treatment, and prevention of nontuberculous mycobacterial diseases," *American Journal of Respiratory and Critical Care Medicine*, vol. 175, no. 4, pp. 367–416, 2007.

[2] D. R. Prevots and T. K. Marras, "Epidemiology of human pulmonary infection with nontuberculous mycobacteria: a review," *Clinics in Chest Medicine*, vol. 36, no. 1, pp. 13–34, 2015.

[3] J. van Ingen, B. E. Ferro, W. Hoefsloot, M. J. Boeree, and D. van Soolingen, "Drug treatment of pulmonary nontuberculous mycobacterial disease in HIV-negative patients: the evidence," *Expert Review of Anti-Infective Therapy*, vol. 11, no. 10, pp. 1065–1077, 2013.

[4] S. Ohshimo, J. Guzman, U. Costabel, and F. Bonella, "Differential diagnosis of granulomatous lung disease: clues and pitfalls: number 4 in the series "Pathology for the clinician" edited by Peter Dorfmüller and Alberto Cavazza," *European Respiratory Review*, vol. 26, no. 145, p. 170012, 2017.

[5] S. J. Hong, T. J. Kim, J.-H. Lee, and J.-S. Park, "Nontuberculous mycobacterial pulmonary disease mimicking lung cancer," *Medicine*, vol. 95, no. 26, p. e3978, 2016.

[6] C. Frehel, C. de Chastellier, T. Lang, and N. Rastogi, "Evidence for inhibition of fusion of lysosomal and prelysosomal compartments with phagosomes in macrophages infected with pathogenic Mycobacterium avium," *Infection and Immunity*, vol. 52, no. 1, pp. 252–262, 1986.

[7] Y. K. Oh and R. M. Straubinger, "Intracellular fate of Mycobacterium avium: use of dual-label spectrofluorometry to investigate the influence of bacterial viability and opsonization on phagosomal pH and phagosome-lysosome interaction," *Infection and Immunity*, vol. 64, no. 1, pp. 319–325, 1996.

[8] C. L. Cosma, O. Humbert, and L. Ramakrishnan, "Superinfecting mycobacteria home to established tuberculous granulomas," *Nature Immunology*, vol. 5, no. 8, pp. 828–835, 2004.

[9] H. E. Volkman, H. Clay, D. Beery, J. C. W. Chang, D. R. Sherman, and L. Ramakrishnan, "Tuberculous granuloma formation is enhanced by a Mycobacterium virulence determinant," *PLoS Biology*, vol. 2, no. 11, article e367, 2004.

[10] J. M. Davis and L. Ramakrishnan, "The role of the granuloma in expansion and dissemination of early tuberculous infection," *Cell*, vol. 136, no. 1, pp. 37–49, 2009.

[11] M. R. Cronan, R. W. Beerman, A. F. Rosenberg et al., "Macrophage epithelial reprogramming underlies mycobacterial granuloma formation and promotes infection," *Immunity*, vol. 45, no. 4, pp. 861–876, 2016.

[12] W. G. Brodbeck and J. M. Anderson, "Giant cell formation and function," *Current Opinion in Hematology*, vol. 16, no. 1, pp. 53–57, 2009.

[13] S. N. Kumar, T. S. Prasad, P. A. Narayan, and J. Muruganandhan, "Granuloma with Langhans giant cells: an overview," *Journal of Oral and Maxillofacial Pathology*, vol. 17, no. 3, pp. 420–423, 2013.

[14] D. Klotz, S. A. Barth, W. Baumgärtner, and M. Hewicker-Trautwein, "*Mycobacterium avium* subsp. *hominissuis* infection in a domestic rabbit, Germany," *Emerging Infectious Diseases*, vol. 24, no. 3, pp. 596–598, 2018.

[15] K. Gharun, J. Senges, M. Seidl et al., "Mycobacteria exploit nitric oxide-induced transformation of macrophages into permissive giant cells," *EMBO Reports*, vol. 18, no. 12, pp. 2144–2159, 2017.

[16] E. Ufimtseva, "*Mycobacterium*-Host Cell Relationships in Granulomatous Lesions in a Mouse Model of Latent Tuberculous Infection," *BioMed Research International*, vol. 2015, Article ID 948131, 16 pages, 2015.

[17] T. Langhans, "XVII. Ueber Riesenzellen mit wandständigen Kernen in Tuberkeln und die fibröse Form des Tuberkels," *Archiv für pathologische Anatomie und Physiologie und für klinische Medicin Band*, vol. 42, pp. 382–404, 1868.

[18] A. K. Lösslein, F. Lohrmann, L. Scheuermann et al., "Monocyte progenitors give rise to multinucleated giant cells," *Nature Communications*, vol. 12, no. 1, p. 2027, 2021.

[19] K. M. Wilburn, R. A. Fieweger, and B. C. VanderVen, "Cholesterol and fatty acids grease the wheels of Mycobacterium tuberculosis pathogenesis," *Pathogens and Disease*, vol. 76, no. 2, 2018.

[20] C. M. McClean and D. M. Tobin, "Early cell-autonomous accumulation of neutral lipids during infection promotes

mycobacterial growth," *PLoS One*, vol. 15, no. 5, article e0232251, 2020.

[21] G. Gago, L. Diacovich, and H. Gramajo, "Lipid metabolism and its implication in mycobacteria-host interaction," *Current Opinion in Microbiology*, vol. 41, pp. 36–42, 2018.

[22] D. A. Keown, *The Role of Cholesterol in the Uptake and Pathogenesis of Mycobacterium avium Subspecies Paratuberculosis in Human Monocytes*, University of Canterbury, 2010.

[23] A. K. Pandey and C. M. Sassetti, "Mycobacterial persistence requires the utilization of host cholesterol," *Proceedings of the National Academy of Sciences of the United States of America*, vol. 105, no. 11, pp. 4376–4380, 2008.

[24] M.-J. Kim, H. C. Wainwright, M. Locketz et al., "Caseation of human tuberculosis granulomas correlates with elevated host lipid metabolism," *EMBO Molecular Medicine*, vol. 2, no. 7, pp. 258–274, 2010.

[25] B. Jeffrey, S. J. Rose, K. Gilbert, M. Lewis, and L. E. Bermudez, "Comparative analysis of the genomes of clinical isolates of Mycobacterium avium subsp. hominissuis regarding virulence-related genes," *Journal of Medical Microbiology*, vol. 66, no. 7, pp. 1063–1075, 2017.

[26] M. Rolando and C. Buchrieser, "A comprehensive review on the manipulation of the sphingolipid pathway by pathogenic bacteria," *Frontiers in Cell and Development Biology*, vol. 7, 2019.

[27] A. Speer, J. Sun, O. Danilchanka et al., "Surface hydrolysis of sphingomyelin by the outer membrane protein Rv0888 supports replication of Mycobacterium tuberculosis in macrophages," *Molecular Microbiology*, vol. 97, no. 5, pp. 881–897, 2015.

[28] A. Lunge, R. Gupta, E. Choudhary, and N. Agarwal, "The unfoldase ClpC1 of *Mycobacterium tuberculosis* regulates the expression of a distinct subset of proteins having intrinsically disordered termini," *The Journal of Biological Chemistry*, vol. 295, no. 28, pp. 9455–9473, 2020.

[29] C. Luberto, M. J. Stonehouse, E. A. Collins et al., "Purification, characterization, and identification of a sphingomyelin synthase from *Pseudomonas aeruginosa*," *The Journal of Biological Chemistry*, vol. 278, no. 35, pp. 32733–32743, 2003.

[30] N. Okino, M. Tani, S. Imayama, and M. Ito, "Purification and characterization of a novel ceramidase from *Pseudomonas aeruginosa*," *The Journal of Biological Chemistry*, vol. 273, no. 23, pp. 14368–14373, 1998.

[31] T. Aronson, A. Holtzman, N. Glover et al., "Comparison of large restriction fragments of Mycobacterium avium isolates recovered from AIDS and non-AIDS patients with those of isolates from potable water," *Journal of Clinical Microbiology*, vol. 37, no. 4, pp. 1008–1012, 1999.

[32] W. M. Matern, J. S. Bader, and P. C. Karakousis, "Genome analysis of *Mycobacterium avium* subspecies *hominissuis* strain 109," *Scientific Data*, vol. 5, no. 1, article 180277, 2018.

[33] S. J. Rose and L. E. Bermudez, "Identification of bicarbonate as a trigger and genes involved with extracellular DNA export in mycobacterial biofilms," *mBio*, vol. 7, no. 6, 2016.

[34] L. Danelishvili, M. J. Poort, and L. E. Bermudez, "Identification of Mycobacterium avium genes up-regulated in cultured macrophages and in mice," *FEMS Microbiology Letters*, vol. 239, no. 1, pp. 41–49, 2004.

[35] J. Wang, X.-L. Pan, L.-J. Ding, D.-Y. Liu, D.-P. Lei, and T. Jin, "Aberrant expression of Beclin-1 and LC3 correlates with poor prognosis of human hypopharyngeal squamous cell carcinoma," *PLoS One*, vol. 8, no. 7, article e69038, 2013.

[36] W. L. Epstein and K. Fukuyama, "Mechanisms of granulomatous inflammation," *Immunology Series*, vol. 46, pp. 687–721, 1989.

[37] S. Mezouar, I. Diarra, J. Roudier, B. Desnues, and J. Mege, "Tumor necrosis factor-alpha antagonist interferes with the formation of granulomatous multinucleated giant cells: new insights into Mycobacterium tuberculosis infection," *Frontiers in Immunology*, vol. 10, 2019.

[38] S. Fais, V. L. Burgio, M. Silvestri, M. R. Capobianchi, A. Pacchiarotti, and F. Pallone, "Multinucleated giant cells generation induced by interferon-gamma. Changes in the expression and distribution of the intercellular adhesion molecule-1 during macrophages fusion and multinucleated giant cell formation," *Laboratory Investigation*, vol. 71, pp. 737–744, 1994.

[39] B. R. Tambuyzer and E. J. Nouwen, "Inhibition of microglia multinucleated giant cell formation and induction of differentiation by GM-CSF using a porcine in vitro model," *Cytokine*, vol. 31, no. 4, pp. 270–279, 2005.

[40] P. J. Brooks, M. Glogauer, and C. A. McCulloch, "An overview of the derivation and Function of multinucleated giant cells and their role in pathologic processes," *The American Journal of Pathology*, vol. 189, no. 6, pp. 1145–1158, 2019.

[41] H. Sakai, I. Okafuji, R. Nishikomori et al., "The CD40–CD40L axis and IFN-γ play critical roles in Langhans giant cell formation," *International Immunology*, vol. 24, no. 1, pp. 5–15, 2012.

[42] D. Glick, S. Barth, and K. F. Macleod, "Autophagy: cellular and molecular mechanisms," *The Journal of Pathology*, vol. 221, no. 1, pp. 3–12, 2010.

[43] S.-W. Kim, B. Subhadra, J. Whang et al., "Clinical Mycobacterium abscessus strain inhibits autophagy flux and promotes its growth in murine macrophages," *Pathogens and Disease*, vol. 75, no. 8, 2017.

[44] I. Iftakhar-E-Khuda, N. Koide, F. Hassan et al., "Novel mechanism of U18666A-induced tumour necrosis factor-α production in RAW 264·7 macrophage cells," *Clinical and Experimental Immunology*, vol. 155, no. 3, pp. 552–558, 2009.

[45] A.-S. Härmälä, M. I. Pörn, P. Mattjus, and J. P. Slotte, "Cholesterol transport from plasma membranes to intracellular membranes is inhibited by 3β-[2-(diethylamino) ethoxy]androst-5-en-17-one," *Biochimica et Biophysica Acta (BBA) - Lipids and Lipid Metabolism*, vol. 1211, no. 3, pp. 317–325, 1994.

[46] A. Meng, C. Luberto, P. Meier et al., "Sphingomyelin synthase as a potential target for D609-induced apoptosis in U937 human monocytic leukemia cells," *Experimental Cell Research*, vol. 292, no. 2, pp. 385–392, 2004.

[47] C. Luberto and Y. A. Hannun, "Sphingomyelin synthase, a potential regulator of intracellular levels of ceramide and diacylglycerol during SV40 transformation:," *The Journal of Biological Chemistry*, vol. 273, no. 23, pp. 14550–14559, 1998.

[48] D. Milhas, N. Andrieu-Abadie, T. Levade, H. Benoist, and B. Ségui, "The tricyclodecan-9-yl-xanthogenate D609 triggers ceramide increase and enhances FasL-induced caspase-dependent and -independent cell death in T lymphocytes," *International Journal of Molecular Sciences*, vol. 13, no. 7, pp. 8834–8852, 2012.

[49] G. Lay, Y. Poquet, P. Salek-Peyron et al., "Langhans giant cells from M. tuberculosis-induced human granulomas cannot

mediate mycobacterial uptake," *The Journal of Pathology*, vol. 211, no. 1, pp. 76–85, 2007.

[50] A. Gasser and J. Möst, "Generation of multinucleated giant cells in vitro by culture of human monocytes with Mycobacterium bovis BCG in combination with cytokine-containing supernatants," *Infection and Immunity*, vol. 67, no. 1, pp. 395–402, 1999.

[51] M.-P. Puissegur, C. Botanch, J.-L. Duteyrat, G. Delsol, C. Caratero, and F. Altare, "An in vitro dual model of mycobacterial granulomas to investigate the molecular interactions between mycobacteria and human host cells," *Cellular Microbiology*, vol. 6, no. 5, pp. 423–433, 2004.

[52] J. M. Anderson, A. Rodriguez, and D. T. Chang, "Foreign body reaction to biomaterials," *Seminars in Immunology*, vol. 20, no. 2, pp. 86–100, 2008.

[53] A. Aghbali, S. Rafieyan, L. Mohamed-Khosroshahi, B. Baradaran, D. Shanehbandi, and M. Kouhsoltani, "IL-4 induces the formation of multinucleated giant cells and expression of β5 integrin in central giant cell lesion," *Medicina Oral, Patología Oral y Cirugía Bucal*, vol. 22, no. 1, pp. e1–e6, 2017.

[54] R. Milde, J. Ritter, G. A. Tennent et al., "Multinucleated giant cells are specialized for complement-mediated phagocytosis and large target destruction," *Cell Reports*, vol. 13, no. 9, pp. 1937–1948, 2015.

[55] J. Braune, A. Lindhorst, J. Fröba et al., "Multinucleated giant cells in adipose tissue are specialized in adipocyte degradation," *Diabetes*, vol. 70, no. 2, pp. 538–548, 2021.

[56] J. Early, K. Fischer, and L. E. Bermudez, "*Mycobacterium avium* uses apoptotic macrophages as tools for spreading," *Microbial Pathogenesis*, vol. 50, no. 2, pp. 132–139, 2011.

[57] H. Clay, J. M. Davis, D. Beery, A. Huttenlocher, S. E. Lyons, and L. Ramakrishnan, "Dichotomous role of the macrophage in early *Mycobacterium marinum* infection of the zebrafish," *Cell Host & Microbe*, vol. 2, no. 1, pp. 29–39, 2007.

[58] S. Sturgill-Koszycki, P. H. Schlesinger, P. Chakraborty et al., "Lack of acidification in Mycobacterium phagosomes produced by exclusion of the vesicular proton-ATPase," *Science*, vol. 263, no. 5147, pp. 678–681, 1994.

[59] L. E. Via, D. Deretic, R. J. Ulmer, N. S. Hibler, L. A. Huber, and V. Deretic, "Arrest of mycobacterial phagosome maturation is caused by a block in vesicle fusion between stages controlled by rab5 and rab7," *The Journal of Biological Chemistry*, vol. 272, no. 20, pp. 13326–13331, 1997.

[60] L. E. M. Bermudez and L. S. Young, "Oxidative and nonoxidative intracellular killing of *Mycobacterium avium* complex," *Microbial Pathogenesis*, vol. 7, no. 4, pp. 289–298, 1989.

[61] C. L. Birmingham, A. C. Smith, M. A. Bakowski, T. Yoshimori, and J. H. Brumell, "Autophagy controls *Salmonella* infection in response to damage to the *Salmonella*-containing vacuole," *The Journal of Biological Chemistry*, vol. 281, no. 16, pp. 11374–11383, 2006.

[62] D.-M. Shin, B.-Y. Jeon, H.-M. Lee et al., "Mycobacterium tuberculosis Eis regulates autophagy, inflammation, and cell death through redox-dependent signaling," *PLoS Pathogens*, vol. 6, no. 12, article e1001230, 2010.

[63] Q. Deng, Y. Wang, Y. Zhang et al., "Pseudomonas aeruginosa triggers macrophage autophagy to escape intracellular killing by activation of the NLRP3 inflammasome," *Infection and Immunity*, vol. 84, no. 1, pp. 56–66, 2016.

[64] C. L. Birmingham, V. Canadien, E. Gouin et al., "Listeria monocytogenes evades killing by autophagy during colonization of host cells," *Autophagy*, vol. 3, no. 5, pp. 442–451, 2007.

[65] S. Steele, J. Brunton, B. Ziehr, S. Taft-Benz, N. Moorman, and T. Kawula, "Francisella tularensis harvests nutrients derived via ATG5-independent autophagy to support intracellular growth," *PLoS Pathogens*, vol. 9, no. 8, article e1003562, 2013.

[66] L. Gerstenmaier, R. Pilla, L. Herrmann et al., "The autophagic machinery ensures nonlytic transmission of mycobacteria," *Proceedings of the National Academy of Sciences of the United States of America*, vol. 112, no. 7, pp. E687–E692, 2015.

[67] M. Knight, J. Braverman, K. Asfaha, K. Gronert, and S. Stanley, "Lipid droplet formation in Mycobacterium tuberculosis infected macrophages requires IFN-γ/HIF-1α signaling and supports host defense," *PLoS Pathogens*, vol. 14, no. 1, article e1006874, 2018.

[68] A. Flieger, F. Frischknecht, G. Häcker, M. W. Hornef, and G. Pradel, "Pathways of host cell exit by intracellular pathogens," *Microbial Cell*, vol. 5, pp. 525–544, 2018.